Hindawi
International Journal of RF and Microwave Computer-Aided Engineering
Volume 2023, Article ID 5240745, 10 pages
https://doi.org/10.1155/2023/5240745

*Research Article*

# A Dual-Band Dual-Output Filtering Power Amplifier Based on High-Selectivity Filtering Impedance Transformer

**Shuchen Zhen**,[1] **Yongle Wu**,[1] **Shaobo Li**,[1] **Zhuoyin Chen**,[1] **and Weimin Wang**[2]

[1]*School of Integrated Circuits, Beijing University of Posts and Telecommunications, Beijing, China*
[2]*School of Electronic Engineering, Beijing University of Posts and Telecommunications, Beijing, China*

Correspondence should be addressed to Yongle Wu; ywu@bupt.edu.cn

Received 3 April 2023; Revised 9 May 2023; Accepted 3 June 2023; Published 15 June 2023

Academic Editor: YongChae Jeong



In this brief, a novel filtering impedance transformer with good selectivity and high termination impedance is proposed, of which close-formed design equations are derived and effectively verified. Then, a dual-band dual-output filtering power amplifier (PA) operating at 2.4-2.6 GHz and 3.4-3.6 GHz is designed based on the proposed filtering impedance transformer. The dual-band filtering PA contains a diplexer-like output matching network, which can separate two band signals into corresponding output branches. EM-simulated results of the diplexer-like output matching network show that the isolation between the two output ports is better than 30.7 dB. Finally, for demonstration, the dual-band dual-output filtering PA using a packaged 10 W transistor is fabricated, and the measured drain efficiencies are 45.3%-50.2% and 41.7%-53.2% at lower and higher bands, respectively. Also, a good dual-band filtering response is obtained. A good agreement between simulated and measured results is observed.

## 1. Introduction

Impedance transformer (IT), as one of the basic components of radio frequency (RF)/microwave systems, can be utilized to achieve the desired impedance matching and the efficient power transmission. To improve the frequency selectivity, various ITs with bandpass response have been widely investigated [1–11] and applied to matching network designs of power amplifiers (PAs) [8–11]. In [1–5], different coupled-line structure filtering impedance transformers (FITs) with ultrahigh transforming ratio realize low/high termination impedance transformations, respectively. Also, cross-shaped [6] and coupled-line structure [7] ITs are presented, both of which can implement an extremely low/high impedance transformation. Furthermore, in [8, 9], FITs with low termination impedance are applied to designs of the input and output matching network (OMN) to achieve codesigns of filtering PAs, respectively.

With the rapid development of 5G communication, RF/microwave components have faced high demands for working at multiple frequencies to improve spectral efficiency. And as a key component of RF/microwave systems, the PA that can operate at multiple frequencies has attracted researchers' attention, such as broadband PAs [12–14] and dual-band PAs [15–19]. Dual-band input matching network (IMN) and OMN are employed to complete designs of dual-band PAs in [15–18]. A dual-band PA, featuring a filter-based input diplexer and a transformer-combined OMN, is designed with two transistors [19]. Meanwhile, applying the dual-output topology to the OMN of PAs is also an effective method to implement the dual-band functionality. And in [20], the dual-output topology can be applied to the scenario of carrier aggregation to improve spectral efficiency. In [20, 21], two dual-band PAs based on the dual-output topology are designed, but they operate within narrow bands and have poor frequency selectivity. Utilizing acoustic wave technology, a dual-band PA with the dual-output topology and a 3% bandwidth is proposed, but it has no physical support, and acoustic wave filters require high processing accuracy [22].

In this brief, a new FIT with high termination impedance is proposed using the coupled-line structure with two loaded stubs. Then, a dual-band filtering PA operating at 2.4-2.6 GHz and 3.4-3.6 GHz is designed based on the proposed

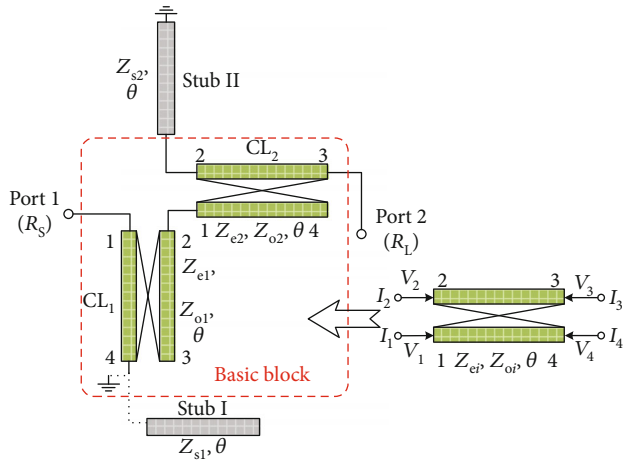


FIGURE 1: The circuit schematic of the proposed filtering impedance transformer.

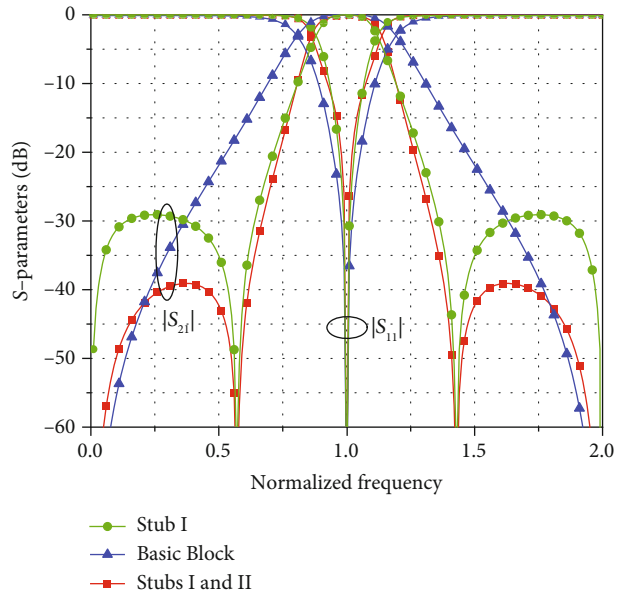


FIGURE 2: Ideal *S*-parameters of the basic block ($C_1 = 0.3$, $Z_o = 40\,\Omega$) and the proposed filtering impedance transformer with the loaded stub I ($Z_{s1} = 90\,\Omega$) and the loaded stub II ($Z_{s2} = 39\,\Omega$).

FIT and the dual-output topology. The diplexer-like OMN can separate signals to corresponding output branches, and a good dual-band filtering preference is demonstrated owing to the use of the FIT. To the authors' knowledge, there are few previous works focused on dual-band PAs with the dual-output topology and the FIT.

## 2. Design Principle of the Filtering Impedance Transformer

Figure 1 shows the circuit schematic of the proposed FIT, which is composed of two cascaded coupled-lines ($CL_1$ and $CL_2$) and two loaded transmission line stubs (stub I and stub II). The basic block with $CL_1$ and $CL_2$ can realize the impedance matching, and the two loaded stubs can improve the selectivity and the stopband rejection of the FIT. Notably, the electrical length $\theta$ is set to 90°, so the loaded stub I with the terminal open should be replaced with the ground in the basic block, and the two loaded stubs would not affect the impedance matching of the basic block. According to the transmission line theory and microwave network analysis [23], the *ABCD* matrix of the basic block with $\theta$ of 90° can be synthesized as follows:

$$\begin{bmatrix} A & B \\ C & D \end{bmatrix}_{\text{Basic block}} = \begin{bmatrix} 0 & \dfrac{jZ_{a1}Z_{b2}}{2Z_{b1}} \\ \dfrac{2jZ_{b1}}{Z_{a1}Z_{b2}} & 0 \end{bmatrix}, \tag{1a}$$

$$\begin{cases} Z_{ai} = Z_{ei} + Z_{oi}, \\ Z_{bi} = Z_{ei} - Z_{oi}, \\ \text{for } i = 1, 2. \end{cases} \tag{1b}$$

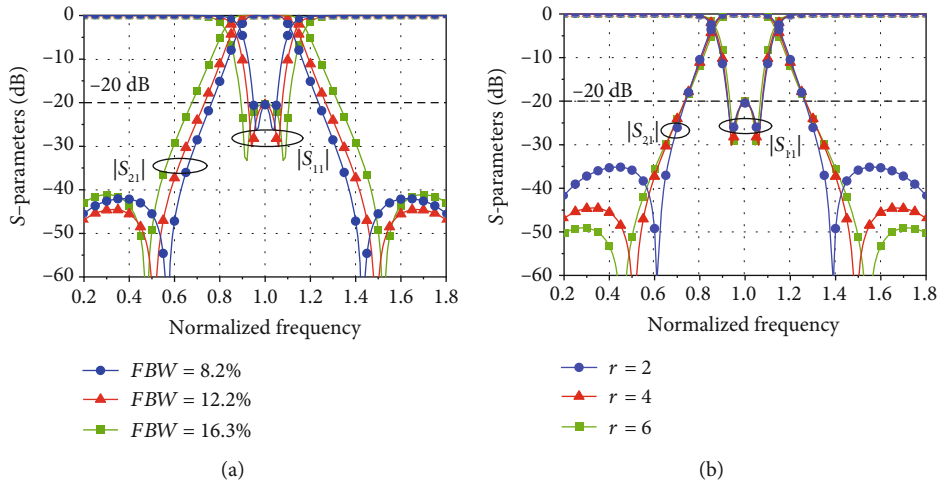


Figure 3: Ideal $S$-parameters of the proposed filtering impedance transformer versus: (a) FBW and (b) $r$.

Table 1: The determined parameters in Figure 3.

| | FBW | RL (dB) | $r$ | $Z_{e1}$ (Ω) | $Z_{o1}$ (Ω) | $Z_{e2}$ (Ω) | $Z_{o2}$ (Ω) | $Z_{s1}$ (Ω) | $Z_{s2}$ (Ω) |
|---|---|---|---|---|---|---|---|---|---|
| Figure 3(a) | 8.2% | 20 | 4 | 87.2 | 51.7 | 91.9 | 45.4 | 107 | 40 |
| | 12.2% | | | 78.2 | 44 | 90.9 | 40 | 65 | 30 |
| | 16.3% | | | 100.2 | 50.5 | 95.9 | 36 | 65 | 35 |
| Figure 3(b) | 12.2% | 20 | 2 | 80.2 | 36 | 89.9 | 41 | 120 | 30 |
| | | | 4 | 78.2 | 44 | 90.9 | 40 | 65 | 30 |
| | | | 6 | 87.2 | 54.1 | 91.9 | 40 | 54 | 33 |

On this basis, the reflection coefficient $S_{11}$ of the basic block can be derived as follows:

$$S_{11} = \frac{Z_{a1}^2 Z_{b2}^2 - 4R_L R_S Z_{b1}^2}{Z_{a1}^2 Z_{b2}^2 + 4R_L R_S Z_{b1}^2}. \tag{2}$$

To achieve the impedance matching at the center frequency $f_0$, the condition that $S_{11}$ is equal to zero needs to be satisfied, and the following result can be obtained:

$$\begin{cases} 2R_L\sqrt{r}C_1 = Z_{e2} - Z_{o2}, \\ C_1 = \dfrac{Z_{e1} - Z_{o1}}{Z_{e1} + Z_{o1}}, \end{cases} \tag{3}$$

where $r$ is the impedance transforming ratio ($= R_S/R_L, R_S > R_L$). To facilitate the determination of circuit parameters, assuming that $Z_{o1} = Z_{o2} = Z_o$ and combined with (3), even-mode impedances of $CL_1$ and $CL_2$ can be calculated as follows:

$$\begin{cases} Z_{e1} = \dfrac{1 + C_1}{1 - C_1} Z_o, \\ Z_{e2} = 2R_L\sqrt{r}C_1 + Z_o. \end{cases} \tag{4}$$

According to (4), once the values of $C_1$ and $Z_o$ are specified, the values of $Z_{e1}$ and $Z_{e2}$ can be calculated. As shown in Figure 2, two additional transmission zeros are obtained by the loaded stub I ($Z_{s1}$) and a better stopband rejection can be achieved by the loaded stub II ($Z_{s2}$), in which characteristic impedances of the two loaded stubs are set as 90 Ω and 39 Ω, respectively. In addition, the values of $C_1$, $Z_o$, $r$, and $R_L$ are set as 0.3, 40 Ω, 4, and 50 Ω, respectively. Two additional transmission zeros (TZs) can be further deduced as

$$\begin{cases} f_{z1} = \dfrac{2f_0}{\pi} \arccos\sqrt{\dfrac{Z_{a1}}{2Z_{s1} + Z_{a1}}}, \\ f_{z2} = \dfrac{2f_0}{\pi}\left(\pi - \arccos\sqrt{\dfrac{Z_{a1}}{2Z_{s1} + Z_{a1}}}\right). \end{cases} \tag{5}$$

From (5), obviously, two additional transmission zeros are only related to the $CL_1$ ($Z_{e1}$, $Z_{o1}$) and the loaded stub I ($Z_{s1}$). Furthermore, to improve the in-band return loss (RL), circuit parameters are optimized, and two transmission poles (TPs) are observed. As shown in Figure 3, to further demonstrate the effectiveness of the proposed FIT, different fractional bandwidths (FBWs) with $r$ fixed to 4 and different $r$ with FBW fixed to 12.2% are implemented,

Table 2: Comparison of filtering impedance transformers.

| Ref. | Termination impedance | TZs | TPs | $r$ | FBWs (%) | CL num.** | Stub num. |
|---|---|---|---|---|---|---|---|
| [3] | High | 4 | 2 | 4/6/8/10 | NA/NA/7.3[a]/NA | 1 | 1 |
| [4] | High | 4 | 3 | 8/10/12 | NA/19[b]/NA | 2 | 1 |
| [5] | Low | 6 | 3 | 5/10 | 19.85[b]/7.96[b] | 1 | 2 |
| [7] | Low/high* | 4 | 2 | 25/71.43 | 5.065[a]/3.25[a] | 1 | 1 |
| [9] | Low | 4 | 3 | 2/5/10 | 22[a]/22[a]/22[a] | 2 | 1 |
| This work | High | 4 | 2 | 2/4/6 | 8.2[a]/12.2[a]/16.3[a] | 2 | 2 |

*Two FITs are designed. [a]20 dB RL. [b]$|S_{11}| > 18$ dB. **The CLs used to realize impedance transformation and the CLs used as stubs are not concluded.

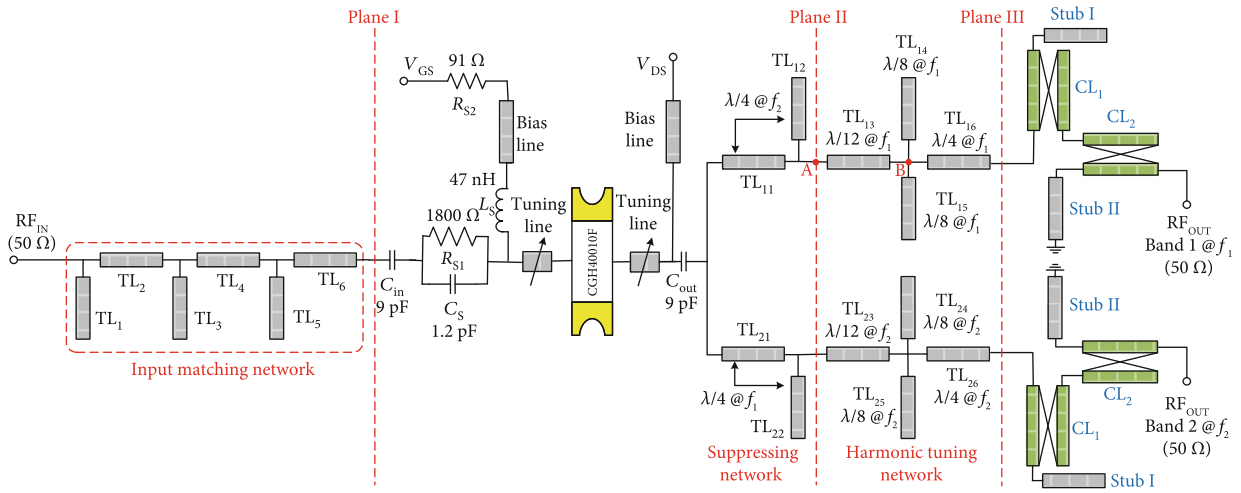


Figure 4: The circuit schematic of the proposed dual-band dual-output filtering power amplifier.

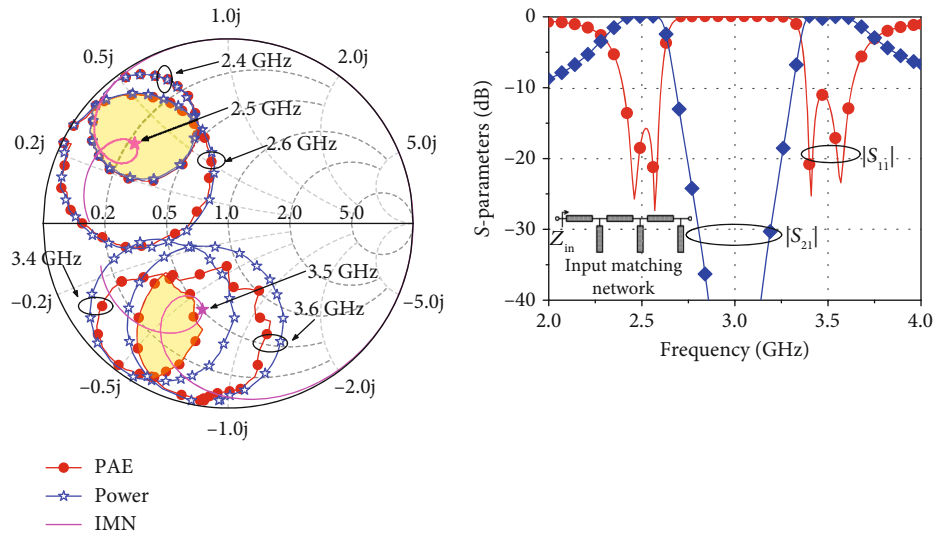


Figure 5: (a) Simulated source-pull contours taken at plane I (see Figure 4) at fundamental frequencies of the CGH40010F device and the trajectory of the input impedance of the input matching network. (b) Ideal $S$-parameters of the input matching network.

while all cases reach a 20 dB in-band RL, and related parameters are summarized in Table 1.

To clarify the differences between this work and the previous works, the comparison of FITs is summarized in Table 2. One coupled-line (CL) and two stubs constitute the FIT to realize the impedance transformation with low termination impedance in [5]. Also, two CLs and one stub are utilized to realize the impedance transformation with

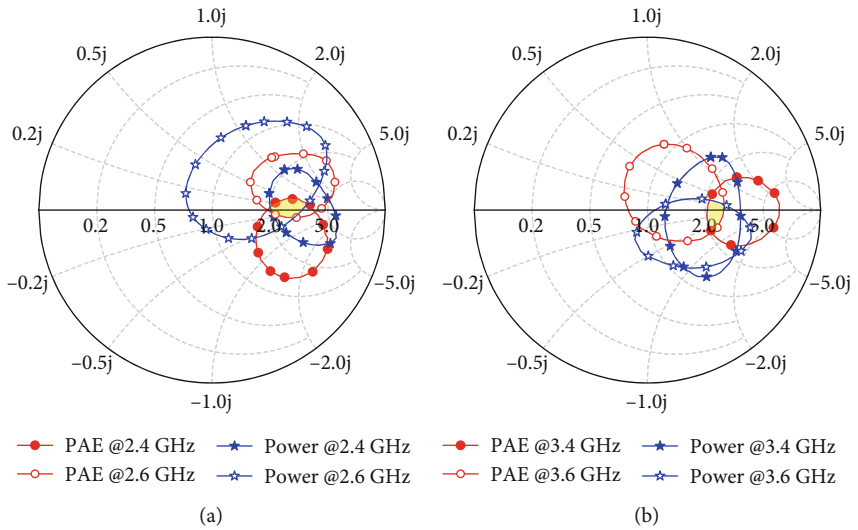


FIGURE 6: Simulated load-pull contours taken at plane III (see Figure 4) at fundamental frequencies for (a) band 1 and (b) band 2 of the CGH40010F device.

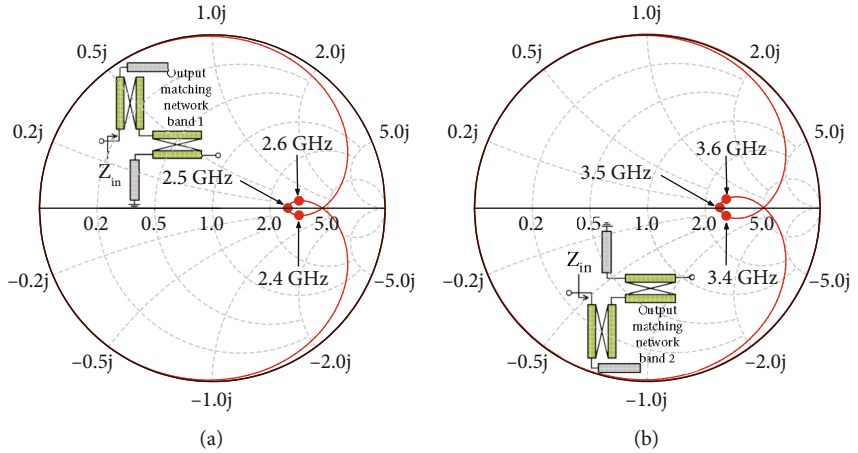


FIGURE 7: Trajectories of input impedances of output matching networks at fundamental frequencies for (a) band 1 and (b) band 2.

low termination impedance in [9]. Then, in [3, 4], two FITs with high termination impedance are proposed. According to the parameters of $r = 4$ given in [3], the spacing gap in the physical size of the CL may be too small and difficult to fabricate, thus limiting its application. The FIT in [4] demonstrates the simulation results of FBWs around 19%; however, it is difficult for the circuit structure to obtain a set of parameters that are convenient for layout in the case of $r = 4$ and FBWs less than 10%, such as the scenario of this work. Next, two FITs with extremely low and high termination impedance are proposed in [7]. For high termination impedance, it is more suitable for situations where $r$ is greater than 50 as shown in [7]. However, the FIT proposed in this work is suitable for situations where $r$ is between 2 and 6, and FBW is approximately between 8% and 16%. Moreover, more degrees of freedom are provided for parameter design, and the obtained parameters are more convenient for layout, due to the use of two CLs for impedance transformation in the FIT of this work.

## 3. Design of the Proposed Dual-Band Dual-Output Filtering PA

The proposed dual-band dual-output filtering PA operating at 2.4-2.6 GHz (band 1) and 3.4-3.6 GHz (band 2) is shown in Figure 4. Center frequencies of the two operating bands are $f_1/f_2$ of band 1/band 2, respectively. $C_{\text{in}}$ and $C_{\text{out}}$ are utilized as DC block to avoid DC signal leakage to RF ports. $R_{S1}$, $C_S$, $R_{S2}$, and $L_S$ constitute the stabilizing circuit. Additionally, the bias circuit entails to provide open-circuited characteristics for both operating bands in the design of the dual-band PA. Two quarter-wavelength transmission lines are used as bias circuits, and their initial parameters are set as 60 Ω and 90° at 3 GHz. With those initial parameters, the input impedances of the bias circuit presented at $f_1/f_2$ are 223 Ω. So, the design of bias circuits has made a compromise between circuit complexity and open-circuited characteristic. Moreover, in order to maximize the efficiency and meet the requirement of the output power for both bands in the

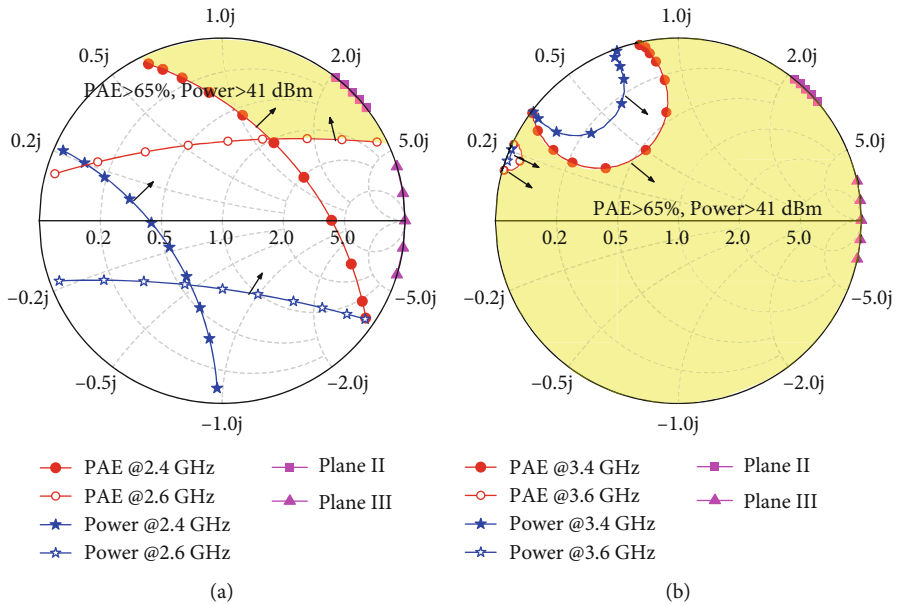


FIGURE 8: Simulated load-pull contours taken at plane II and trajectories of input impedances taken at plane II and plane III (see Figure 4), at second-order harmonic frequencies for (a) band 1 and (b) band 2 of the CGH40010F device.

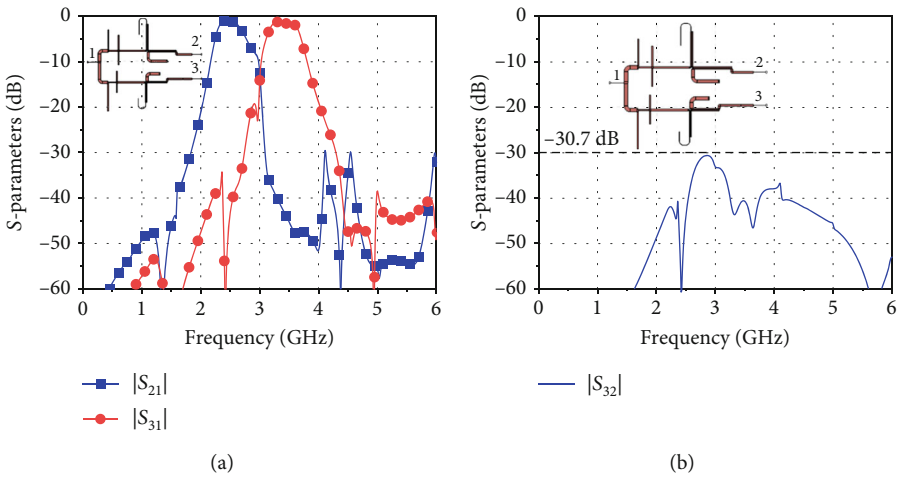


FIGURE 9: EM-simulated results of the diplexer-like output matching network for (a) $|S_{21}|$ and $|S_{31}|$ and (b) $|S_{32}|$.

process of load-pull taken at plane II, parameters of the output bias line are optimized as 60 Ω and 86° at 3.4 GHz.

The suppressing network of each branch consists of two transmission lines with an electrical length of 90° at the center frequency of the other band, which can present a high impedance characteristic to the other branch to suppress the signal transmission of the other band. Besides, to improve the power transmission efficiency, harmonic tuning networks are added to the schematic. For band 1, $TL_{14}$ and $TL_{15}$, two loaded eighth-wavelength open-circuited stubs operating at $f_1$, are utilized to short-circuit the second-order harmonic impedance at point *B*. It is found that using two loaded eighth-wavelength open-circuited stubs can better suppress out-of-band spurious signals in the small-signal results of the PA through simulation. Thus, two loaded eighth-wavelength open-circuited stubs are utilized in the design of the PA. And the cascaded twelfth-wavelength transmission line $TL_{13}$ operating at $f_1$ can transfer the second-order harmonic impedance to the optimal impedance region at point *A*. For band 2, the same analysis can be performed. Notably, the designs of the suppressing network and the harmonic tuning network are referred to [21]. To obtain the filtering characteristic to improve the frequency selectivity, the proposed FIT is applied to the design of the PA, and a quarter-wavelength transmission line $TL_{16}$ ($TL_{26}$) operating at $f_1$ ($f_2$) can convert the low impedance to the high impedance.

In Figure 5(a), source-pulls taken at plane I at fundamental frequencies for each band are implemented, and the trajectory of the input impedance of the IMN is near

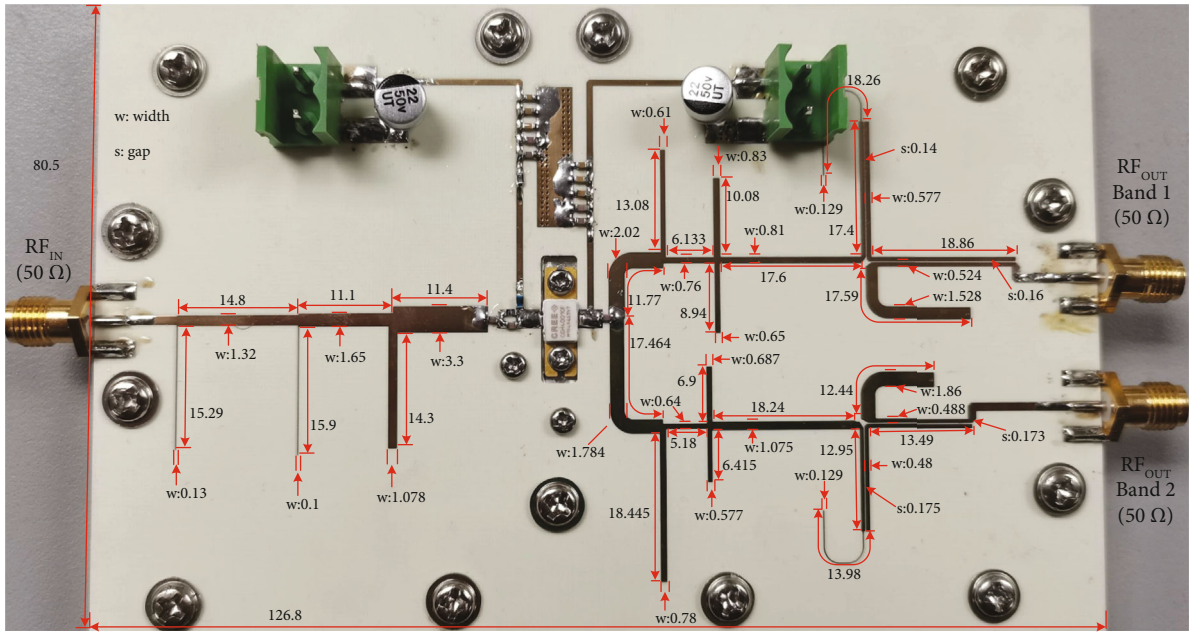


Figure 10: Photograph of the fabricated dual-band dual-output filtering power amplifier with its main dimensions (unit: mm).

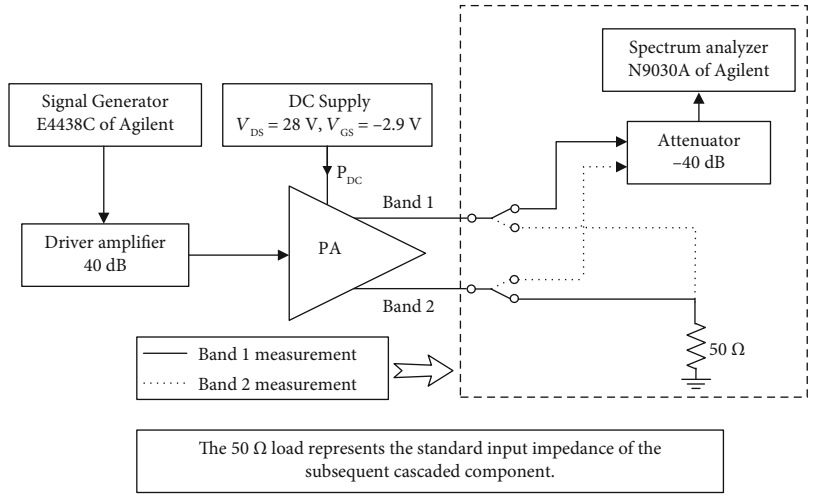


Figure 11: Experimental measurement flow diagram and related setups.

the overlapping area for each band. Then, the classic three-segment series parallel transmission line structure is utilized to achieve the dual-band input matching. The design of the IMN is referred to [16], and good impedance matchings for each band are achieved as shown in Figure 5(b). In Figure 6, load-pulls taken at plane III at fundamental frequencies for each band are implemented, and according to overlapping areas (power added efficiency (PAE) > 60% and output power > 40 dBm), fundamental load impedances at plane III are selected as 150/120 Ω for band 1/band 2, respectively. After, OMNs for each band are designed based on load-pull results and the proposed FIT as shown in Figure 7. Besides, harmonic tuning networks are added to the schematic, and input impedances taken at plane II at second-order harmonic frequencies are located at overlapping areas (PAE > 65% and output power > 41 dBm) for each band as shown in Figure 8.

Moreover, EM simulation is employed to the diplexer-like OMN with a dual-band filtering characteristic and an isolation better than 30.7 dB as shown in Figure 9. And insertion losses at center frequencies of two passbands are 1.13 dB and 1.66 dB, respectively.

## 4. Fabrication and Experimental Results

Finally, as shown in Figures 10 and 11, the proposed dual-band dual-output filtering PA is fabricated and measured on the Rogers 4350B substrate with a relative permittivity of 3.66, a loss tangent of 0.0035, and a thickness of 0.508 mm. A 10 W Cree Wolfspeed CGH40010F transistor

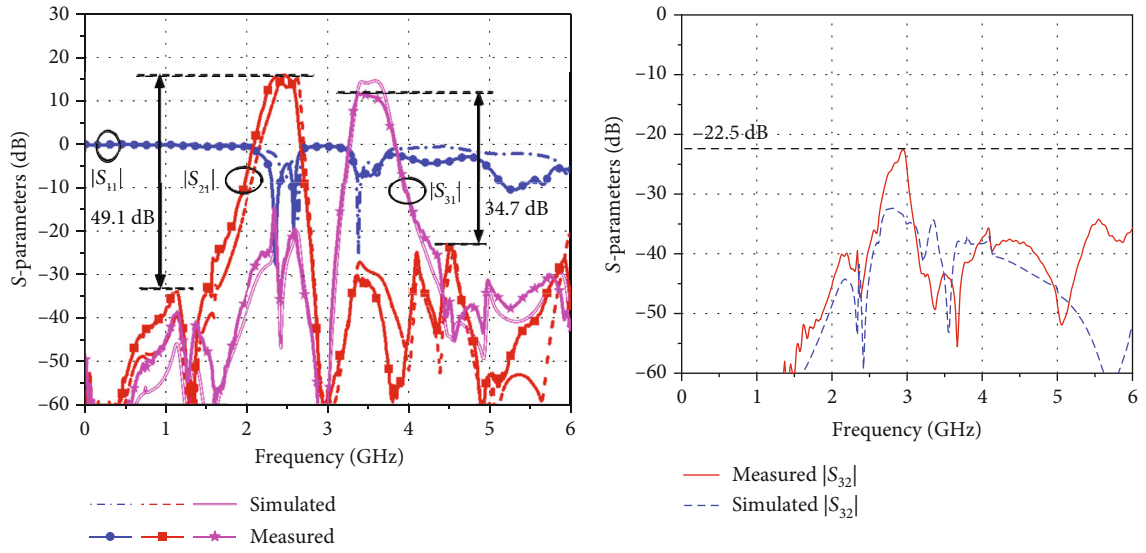


FIGURE 12: EM-simulated and measured small-signal *S*-parameters, (a) $|S_{11}|$, $|S_{21}|$, and $|S_{31}|$ and (b) $|S_{32}|$, of the proposed dual-band dual-output filtering power amplifier.

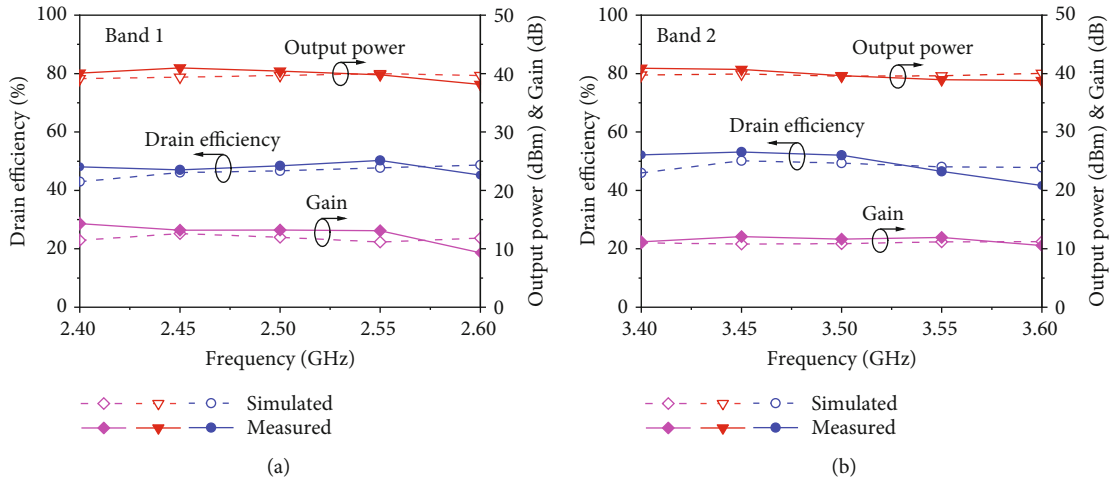


FIGURE 13: EM-simulated and measured large-signal results of the proposed dual-band dual-output filtering power amplifier versus frequency at (a) band 1 and (b) band 2.

is used, of which the gate voltage is -2.9 V and the drain voltage is 28 V with the quiescent current of 106 mA. Notably, the output port of band 2 is connected with a 50 Ω load standard part when conducting the large-signal measurement for band 1 as shown in Figure 11. The 50 Ω load standard part represents the standard input impedance of the subsequent cascaded component, so the accuracy of test results can be guaranteed.

Figure 12(a) depicts a good dual-band filtering characteristic with high selectivity at each band. Measured small-signal gains at center frequencies of two passbands are 13.1 dB and 10.9 dB, respectively. Measured lower and upper stopband rejections are better than 49.1 dB (DC-1.32 GHz) and 34.7 dB (4.51-6 GHz), respectively. In Figure 12(b), the isolation between two output ports is better than 22.5 dB. Besides, Figure 13 presents large-signal measurement results of each band, of which drain efficiencies (DEs) are 45.3%-50.2% and 41.7%-53.2% at band 1 and band 2, respectively. Output powers are 38.1-41 dBm and 38.8-40.9 dBm at band 1 and band 2, respectively. For band 1, within the passband from 2.4 to 2.55 GHz, the output power is better than 39.8 dBm. For band 2, within the passband from 3.4 to 3.5 GHz, the output power is better than 39.6 dBm.

Additionally, to evaluate the performance of the linearized dual-band dual-output filtering PA, tests are implemented for each band with a 20 MHz, 7 dB peak-to-average power ratio (PAPR) and long-term evolution (LTE) signal, while the PA operates in the single band at each center frequency. As shown in Figures 14(a) and 14(b), when digital predistortion (DPD) is applied to the PA, an adjacent

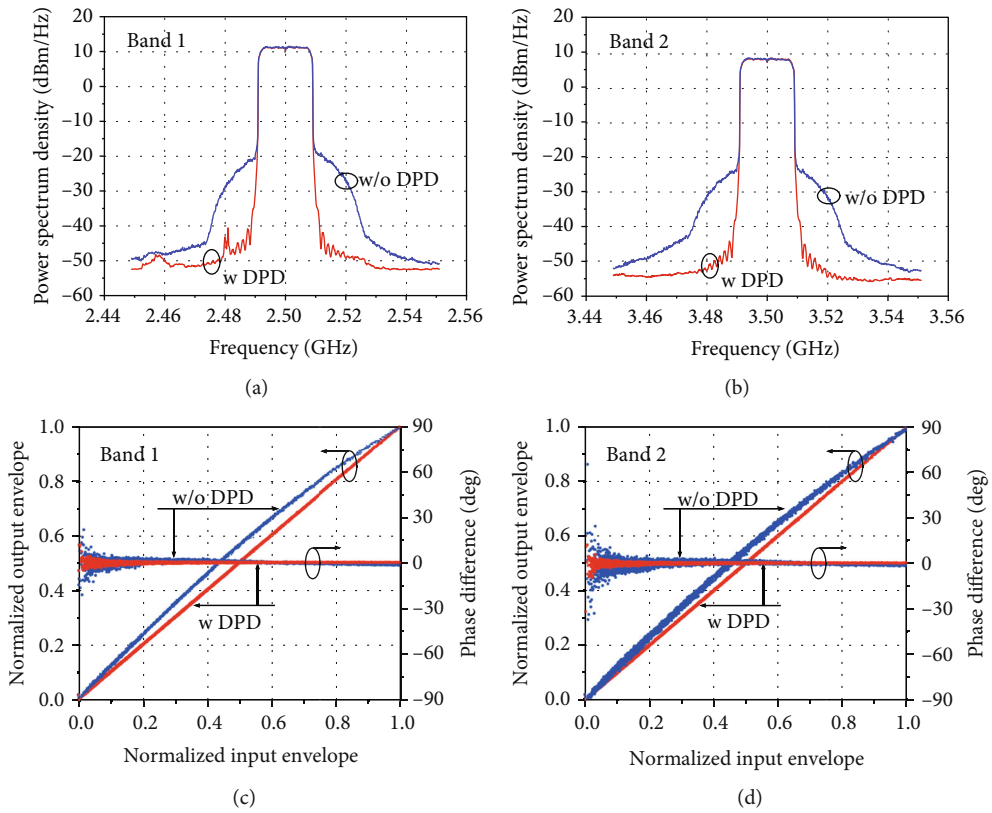


FIGURE 14: Measured power spectrum density with and without DPD at (a) band 1 and (b) band 2. AM/AM and AM/PM distortion characteristics, with and without DPD, at (c) band 1 and (d) band 2.

TABLE 3: Performance comparison of the dual-band dual-output PAs.

| Ref. | $f_1/f_2$ (GHz) | FBWs (%) | Efficiency (%) | $P_{out}$ (dBm) | Technology | Filtering |
|---|---|---|---|---|---|---|
| [20] | 3.4/5.5* | 4.4/4.5* | 40.4/39.9[a] | 36.7/37.1 | Microstrip | No |
| [21] | 3.5/5 | 5.7/4* | 55.8/53.8[b] | 40.2/40.7 | Microstrip | No |
| [22]** | 2.535/2.63 | 3/3 | 52.4/57.2[a] | 38.43/37.6 | Acoustic wave | Yes |
| This work | 2.5/3.5 | 8/5.7 | 50.2/53.2[b] | 41/40.9 | Microstrip | Yes |

[a]The maximum power added efficiency. [b]The maximum drain efficiency. $P_{out}$: the maximum output power. *Based on measured large-signal results. ** Without physical support.

channel power ratio (ACPR) of -57.62/-57.64 dBc is obtained at two bands, respectively. AM/AM and AM/PM characteristics with and without DPD are shown in Figures 14(c) and 14(d).

Generally, measured results are in a good agreement with EM-simulated results, and performance comparisons for PAs with the dual-output topology are summarized in Table 3. In [20, 21], two dual-band dual-output PAs operating at two single frequency points are designed. And their FBWs are estimated from the measured large-signal results because overall small-signal results of PAs are not provided. In [20], FBW is calculated when the gain of the PA decreases by 1 dB, but the PAE drops sharply from the center frequency to both sides at the two bands, which will limit its applications to practical scenarios. In [21], FBW is estimated when the DE is greater than 40%; however, the curves of gain and output power versus frequency are not flat within the estimated FBW. Both PAs mentioned above do not show filtering characteristics. In [22], a dual-band dual-output filtering PA is designed utilizing acoustic wave filters, and the simulated small-signal result shows a 3% FBW at two bands, while it has no physical support. In this work, a dual-band dual-output PA with the filtering characteristic is designed and fabricated, and a 200 MHz bandwidth of each band is obtained from the measured small-signal result. Meanwhile, DE, gain, and output power of each band are relatively flat observed from the measured large-signal result.

## 5. Conclusion

In this brief, a novel FIT is proposed and detailed design equations are provided. Then, the FIT is applied to the design of the dual-band dual-output filtering PA, with the dual-output topology and a diplexer-like OMN. The

proposed PA operating at 2.4-2.6/3.4-3.6 GHz is simulated, fabricated, and measured. An excellent dual-band filtering characteristic with high selectivity is observed from measured small-signal results.

## Data Availability

The data that support the findings of this study are available on request from the corresponding author. The data are not publicly available due to privacy or ethical restrictions.

## Conflicts of Interest

The authors declare that they have no conflicts of interest.

## Acknowledgments

This work was supported by the National Natural Science Foundations of China (nos. 61971052, U21A20510, and U20A20203).

## References

[1] P. Kim, G. Chaudhary, and Y. Jeong, "Ultra-high transforming ratio coupled line impedance transformer with bandpass response," *IEEE Microwave and Wireless Components Letters*, vol. 25, no. 7, pp. 445–447, 2015.

[2] Q.-S. Wu and L. Zhu, "Short-ended coupled-line impedance transformers with ultrahigh transforming ratio and bandpass selectivity suitable for large load impedances," *IEEE Transactions on Components, Packaging and Manufacturing Technology*, vol. 6, no. 5, pp. 767–774, 2016.

[3] P. Kim and Y. Jeong, "A coupled line impedance transformer for high termination impedance with a bandpass filtering response," *Journal of Electromagnetic Engineering and Science*, vol. 18, no. 1, pp. 41–45, 2018.

[4] S. Chen, M. Li, Y. Yu, and M. Tang, "A filtering impedance transformer with high transforming ratio," *Microwave and Optical Technology Letters*, vol. 60, no. 8, pp. 1869–1872, 2018.

[5] P. Kim and Y. Jeong, "High selectivity and wideband bandpass filtering impedance transformer," *International Journal of RF and Microwave Computer-Aided Engineering*, vol. 31, no. 3, 2021.

[6] H.-X. Zhu, P. Cheong, S.-K. Ho, K.-W. Tam, and W.-W. Choi, "Realization of extremely high and low impedance transforming ratios using cross-shaped impedance transformer," *IEEE Transactions on Circuits and Systems II: Express Briefs*, vol. 67, no. 7, pp. 1189–1193, 2020.

[7] Y. Jeong, G. Chaudhary, and P. Kim, "Frequency selective impedance transformer with high-impedance transforming ratio and extremely high/low termination impedances," *IEEE Transactions on Circuits and Systems I: Regular Papers*, vol. 68, no. 6, pp. 2382–2392, 2021.

[8] Z. Su, C. Yu, B. Tang, and Y. Liu, "Bandpass filtering power amplifier with extended band and high efficiency," *IEEE Microwave and Wireless Components Letters*, vol. 30, no. 2, pp. 181–184, 2020.

[9] Z. Zhuang, Y. Wu, M. Kong, and W. Wang, "High-selectivity single-ended/balanced DC-block filtering impedance transformer and its application on power amplifier," *IEEE Transactions on Circuits and Systems I: Regular Papers*, vol. 67, no. 12, pp. 4360–4369, 2020.

[10] J.-X. Xu, X. Y. Zhang, and X.-Q. Song, "High-efficiency filter-integrated class-F power amplifier based on dielectric resonator," *IEEE Microwave and Wireless Components Letters*, vol. 27, no. 9, pp. 827–829, 2017.

[11] Q.-Y. Guo, X. Y. Zhang, J.-X. Xu, Y. C. Li, and Q. Xue, "Bandpass class-F power amplifier based on multifunction hybrid cavity–microstrip filter," *IEEE Transactions on Circuits and Systems II: Express Briefs*, vol. 64, no. 7, pp. 742–746, 2017.

[12] Z. Zhuang, Y. Wu, Q. Yang, M. Kong, and W. Wang, "Broadband power amplifier based on a generalized step-impedance quasi-Chebyshev lowpass matching approach," *IEEE Transactions on Plasma Science*, vol. 48, no. 1, pp. 311–318, 2020.

[13] Y. Jian, G. Liu, Z. Cheng, Z. Zhao, and W. Wang, "Compact broadband high-efficiency power amplifier using terminated coupled line filter matching network," *International Journal of RF and Microwave Computer-Aided Engineering*, vol. 31, no. 11, article e22815, 2021.

[14] A. S. I. Amar, M. Mamidanna, M. Darwish, and H. El-Hennawy, "High gain broadband power amplifier design based on integrated diplexing networks," *IEEE Microwave and Wireless Components Letters*, vol. 32, no. 2, pp. 133–136, 2022.

[15] Y. Wang and Y. C. Li, "Single- and dual-band filtering power amplifiers," in *2020 IEEE MTT-S International Microwave Workshop Series on Advanced Materials and Processes for RF and THz Applications (IMWS-AMP)*, pp. 1–3, Suzhou, China, 2020.

[16] X. Gui, C. Yu, S. Li, M. Su, and Y. Liu, "Design of dual-band power amplifier based on band-stop input matching structure," in *2021 IEEE Asia-Pacific Microwave Conference (APMC)*, pp. 488–490, Brisbane, Australia, 2021.

[17] Z. Zhang, Z. Cheng, V. Fusco, and C. Gu, "Design of a dual-band power amplifier using a simple method," *IEEE Microwave and Wireless Components Letters*, vol. 31, no. 2, pp. 149–152, 2021.

[18] H. Zhao, Y. Wu, W. Wang, and Y. Liu, "A novel dual-band highly efficient power amplifier for 5G applications," *International Journal of RF and Microwave Computer-Aided Engineering*, vol. 32, no. 5, article e23093, 2022.

[19] H. Tao, J. Wang, Y. Wang et al., "High-power Ka/Ku dual-wideband GaN power amplifier with high input isolation and transformer-combined load design," *IEEE Microwave and Wireless Components Letters*, vol. 31, no. 1, pp. 49–51, 2021.

[20] T. Cappello, A. Duh, T. W. Barton, and Z. Popovic, "A dual-band dual-output power amplifier for carrier aggregation," *IEEE Transactions on Microwave Theory and Techniques*, vol. 67, no. 7, pp. 3134–3146, 2019.

[21] X. Chen, Y. Wu, and W. Wang, "Dual-band, dual-output power amplifier using simplified three-port, frequency-dividing matching network," *Electronics*, vol. 11, no. 1, p. 144, 2022.

[22] P. Silveira, J. Verdú, and P. De Paco, "Dual-band dual-output codesigned power amplifier in acoustic wave technology," in *2021 IEEE International Ultrasonics Symposium (IUS)*, pp. 1–4, Xi'an, China, 2021.

[23] D. M. Pozar, *Microwave Engineering*, John Wiley & Sons, Hoboken, NJ, USA, 4th ed. edition, 2012.